J. Fluid Mech. (1997), *vol.* 349, *pp.* 361–380. Printed in the United Kingdom

On the nonlinear Helmholtz response of almost-enclosed tidal basins with sloping bottoms

By LEO R. M. MAAS

Netherlands Institute for Sea Research, PO Box 59, 1790 AB Texel, The Netherlands
e-mail: maas@nioz.nl

(Received 24 October 1996 and in revised form 9 June 1997)

Short relatively deep tidal basins, which are connected to the open sea by a narrow strait, may exhibit either an amplified (resonant), or damped (choked) response to the tide at the entrance. Here particular attention is given to the lowest mode of response, which is the Helmholtz or pumping mode, for which the sea level within the basin executes a spatially uniform oscillation. When the basin's sidewalls slope, the restoring process of this oscillator is nonlinear. Possible consequences of this nonlinearity are that the basin may exhibit either long-lasting high-waters and short, peaked low-waters or long-term regular modulation of its tidal amplitude, or a chaotic modulation of its tidal amplitude, or 'bent resonance horns', implying that resonant and choked tidal responses may exist simultaneously for the same parameter regime. Related field observations will be discussed.

1. Introduction

Tides have a strong impact on the coastal environment. Not only can tides affect rivers over very long distances, like in the Amazon, where their influence is marked up to 850 km from the mouth of the river (Defant 1961), but their effects become even more dramatic in coastal embayments, where the tide can be significantly amplified, up to a range of 17 m in the Bay of Fundy (Garrett 1972), due to the proximity of one of its key frequencies to one of the eigen-frequencies of the bay.

Different geometric settings of coastal waters determine different kinds of responses, which need their own description of the physics involved. In the first example above, for instance, the tide, 'propagating' up-river, is of a *diffusive* nature, due to the balance between pressure gradient and quadratic bottom friction which exists in the (along-river) momentum equation (LeBlond 1978; Friedrichs & Madsen 1992). The tidal influence thus gradually diminishes up-river. In contrast, in the second example, inertial effects *are* relevant, and lead to resonant amplification of the tide. A finite-amplitude response is in this case mainly due to radiative damping of the resonating bay, a linear damping mechanism (Garrett 1975).

Relatively wide coastal embayments are, like organ pipes, mostly dominated by quarter-wave resonances. In short deep basins, connected to the open sea by a narrow strait, a still simpler kind of resonance may be produced by an oscillatory external tide: the Helmholtz mode (Mei 1989). This mode can be best understood as a perturbation of an enclosed basin. An enclosed basin has eigenmodes which are all characterized by the fact that they necessarily conserve mass. Thus, there will always be a zero-elevation line somewhere in the basin, which seperates regions with opposite phases

(180° phase difference). These eigenmodes are therefore aptly referred to as sloshing modes. The sole mode added to this system when the basin communicates with a tidal sea through a narrow strait is the *pumping* or Helmholtz mode, characterized by a periodic mass exchange through the narrows and associated spatially uniform elevation change within the basin. This is generally also the most energetic mode of such a basin (Carrier, Shaw & Miyata 1971). The Helmholtz mode has been employed to explain tidal oscillations in, for instance, Lake Maracaibo (Redfield 1961; Molines, Fornerino & LeProvost 1989), and even in a system as big as the Gulf of Mexico in order to explain the relatively large amplitudes of its diurnal tides (Platzman 1972). Incidentally, this mode need not necessarily be excited by an oscillatory external flow as it may also be produced by a steady shear current at its entrance (Fabrikant 1995).

The linear Helmholtz oscillator is well-known in tidal analysis, albeit on a much smaller scale and, actually, not as a resonator, but as a damper. It happens to describe also the response of a 'stilling well', a device which measures tidal height in a cylinder which is connected to the open sea by a submerged small tube, which is constructed precisely to filter out high-frequency wind and capillary waves, see Shih & Baer (1991). Thus, the linear response of an almost-enclosed basin to a tide in the connecting sea can be two-fold. Either the tide is amplified, as when the basin is near resonance, or it is suppressed – 'choked' (Stigebrandt 1980), far away from resonance. Clearly this is not only determined by the near-resonance of the forcing frequency, but also by the strength of the damping. Here damping is, apart from radiative losses alluded to before, controlled by two processes in the strait. The first process is quadratic bottom friction of the strong currents in the narrows – frictional loss in the basin being small due to the relative weakness of the currents there (Mehta & Özsoy 1978; Zimmerman 1992). The second process is due to the asymmetry of the calm spread-out inflow and the swift jet-like outflow (Stommel & Farmer 1953), which produces a difference in dynamic pressure (Bernoulli head) between entrance and exit, reducing the total head (pressure difference) driving the flow through the channel. Remarkably, these two processes lead to the same nonlinear quadratic damping law, see Mehta & Özsoy (1978).

The frictional, Helmholtz or cavity resonator, derived in §2, is an attractive model of tides in almost-enclosed basins because it captures much of the essential physics, while retaining the simplicity of a lumped-parameter model (Elmore & Heald 1969). One aspect notably absent in the usual application of this model, however, is a proper description of the geometry of the basin. It is common that in these kinds of models the basin is supposed to have vertical sidewalls (see §3). In reality sidewalls are sloping, in particular for tidal basins possessing extensive tidal flats, like for instance those of the Wadden Sea – a complex of tidal basins, separated by tidal flats and watersheds, see figure 1. Although drying banks have routinely been incorporated in numerical models (e.g. Flather & Heaps 1975; Speer & Aubrey 1985) their study, from a fundamental point of view, has been relatively neglected. The effect of a sloping sidewall on the period of a Helmholtz resonator has recently been addressed by Green (1992), who formulated an unforced inviscid small-amplitude version of the evolution equation to be discussed here. He showed that by including sloping sidewalls the Helmholtz oscillator becomes nonlinear and by perturbation methods found that the period of its free Helmholtz mode diminishes slightly with increasing amplitude of the response. In §4 the finite-amplitude response of the free as well as the forced and damped nonlinear Helmholtz oscillator will be addressed, both analytically and numerically. The nonlinearity will be shown to lead to a distortion of the tidal profile, to slow modulation of the tidal amplitude, possibly to chaotic tides, and, for the most realistic situation which includes both forcing and damping,

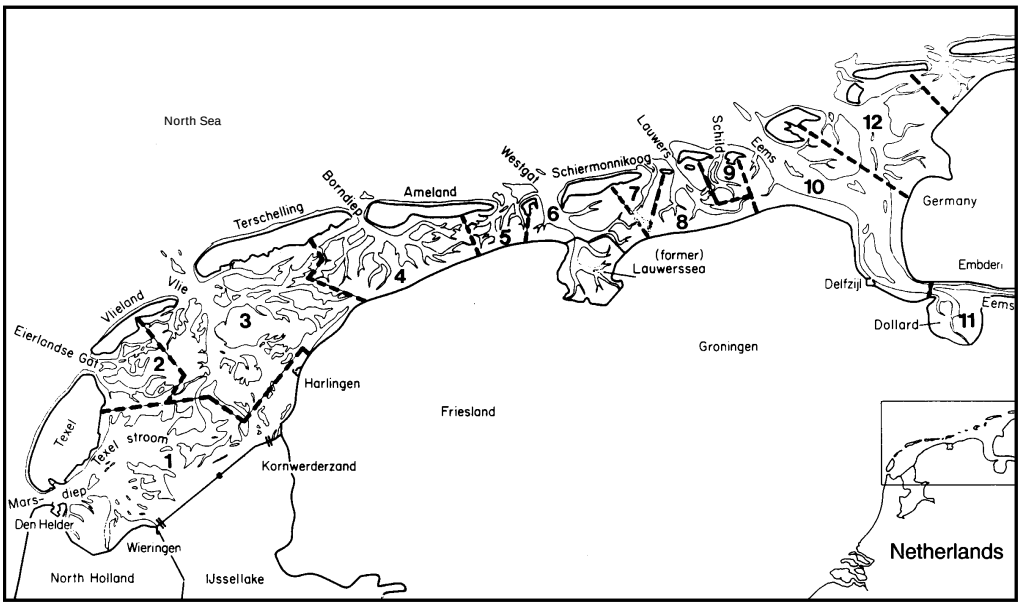

FIGURE 1. Bathymetric chart of the Dutch part of Wadden Sea, with watersheds dashed. Isobaths (thin solid lines) refer to mean sea level. Numbers refer to basins, the names and characteristic dimensions of which are given in table 1.

to multiple equilibria. The latter indicates that a basin may exhibit, under certain circumstances, both an amplified and a choked tidal regime, which may, in principle, lead to a dramatic change in tidal range under a small variation of the environmental parameters. In this section also the possible relevance of this model to tides in the Wadden Sea will be discussed. In §5 the paper is summarized and some unresolved aspects of the problem are discussed.

2. Tidal Helmholtz resonator

Consider a basin with top view as sketched in Figure 2, of maximum depth H and horizontal area A_*, which depends on depth z_*/H, and which is connected to the sea by a narrow strait of width B and depth H. The vertical coordinate z_* is measured from mean-water level upwards. Assume that the strait's length L, as well as the basin's length scale $A_0^{1/2}$, are much smaller than the tidal wavelength in the basin, λ, so that the tidal wave traverses the basin 'instantaneously'. Here $A_0 = A_*(0)$ is the basin's surface area at $z_* = 0$ in the absence of an external tide. The tidal wavelength $\lambda = 2\pi c/\sigma_e$ is determined by the lunar semi-diurnal tidal frequency $\sigma_e = 1.4 \times 10^{-4}$ rad s^{-1} and the long-wave speed $c = (gH)^{1/2}$, in which g denotes the acceleration due to gravity. Let the external (tidal) elevation at sea $\zeta_e(\sigma_e t_*)$ be a given periodic function of time t_*. Then, when the basin is relatively broad and thus velocities and frictional effects small, the momentum equations within the basin reduce, to lowest order, to a statement that horizontal pressure gradients (and thus also horizontal gradients in the elevation field) vanish. The response within the basin will therefore be dominated by the spatially uniform Helmholtz mode. The state of the tide within the basin can then simply be described by a single time-dependent parameter, like the surface elevation, ζ_i, or the volume. Here we will actually employ the *excess* volume

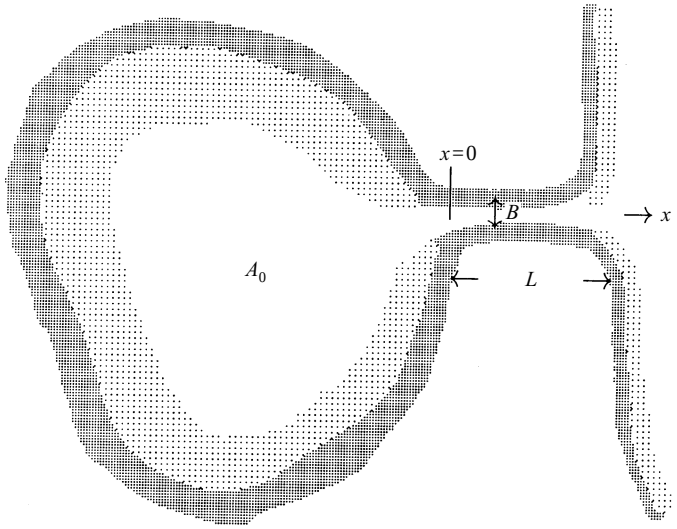

FIGURE 2. Definition sketch of a tidal basin with connecting strait.

within the basin, $V_* \equiv \int_0^{\zeta_i} A_*(z_*/H)\mathrm{d}z_*$, which is the amount of fluid in excess of the volume contained in the basin below mean sea level. The excess volume within the basin changes due to the mass flux entering through the strait

$$\frac{\mathrm{d}V_*}{\mathrm{d}t_*} = -u_0(H+\zeta_0)B. \tag{1}$$

Here $u(x,t_*)$ is the depth-averaged flow (aligned in the along-strait x-direction) and $\zeta_*(x,t_*)$ the surface elevation within the strait. Subscripts 0 refer to the values these variables take at the entrance of the basin ($x = 0$). The flow through the strait, neglecting Coriolis effects, is determined by the momentum equation

$$\frac{\partial u}{\partial t_*} = -\frac{\partial}{\partial x}(g\zeta_* + \tfrac{1}{2}u^2) - \frac{k}{H+\zeta_*}|u|u, \tag{2}$$

where k is a bed stress coefficient ($k \approx 0.0025$). The dynamic pressure term (second term on the right) may contain an additional multiplication factor, reflecting the depth-dependence of the real flow, omitted here (Prandle 1991). Several simplifying assumptions are made. The flow within the channel is assumed to be uniform in the downstream (and cross-stream) direction $u_0 \equiv u(t_*)$, the change in the flow field, in response to a dramatic change in width, at both ends taking place just outside the strait. Similarly, the elevation is assumed to drop linearly over the length of the channel. Consistency requires the surface elevation to be negligible when compared to the mean channel depth, both in the expression for the mass flux on the right-hand side of (1), and in the denominator on the right-hand side of (2). This is physically equivalent to the assumption that the strait is approximated by a *pipe* and is simply driven by the pressure difference $g(\zeta_e - \zeta_i)$, where subscripts i, e refer to values of the variables just in the interior (basin) and exterior (sea) respectively. Therefore, integrating (2) along the length of the channel, L, from just inside the basin at $x = 0^-$ (where $\zeta_* = \zeta_i$) to just outside the channel at $x = L^+$ (where $\zeta_* = \zeta_e$), and neglecting the above terms, leads to

$$L\frac{\mathrm{d}u}{\mathrm{d}t_*} = g(\zeta_i - \zeta_e) + \tfrac{1}{2}(u_i^2 - u_e^2) - L\frac{k}{H}|u|u, \tag{3}$$

while the change in excess volume is now simply given by

$$\frac{\mathrm{d}V_*}{\mathrm{d}t_*} = -uHB. \tag{4}$$

The difference in the jet-like outflow and the potential-flow-like inflow implies that the dynamic pressure difference (the second term on the right of (3)) can be evaluated as follows. Consider the ebb flow ($u > 0$). In this case the widespread inflow is less than the channel flow (but still proportional to it): $u_i = (1-\delta)u < u$, where δ denotes an empirical proportionality constant. However, the outflow, initially at least, retains its width as a jet and therefore has approximately $u_e = u$. Hence, for small values of δ, $0 < \delta \ll 1$, the difference in dynamic pressure is $-\delta u^2$. In the flood phase ($u < 0$) $u_i = u$, and $u_e = (1-\delta)u$, so that this difference amounts to δu^2. In general, therefore, the dynamic pressure difference is $-\delta|u|u$, and has a form analogous to the bottom-friction term (last term of (3)), with which it is combined below.

Bottom friction and the pressure drop related to the asymmetry between in- and outflow are not the only processes damping the Helmholtz oscillator. When the sea-level oscillation within the basin is amplified with respect to its value at sea the basin will lose some energy by radiating waves back into the sea. This leads to a number of adjustments to the above expressions (Miles 1948; Garrett 1975). First, because part of the water outside the strait now takes part in the oscillation, the effective length of the channel L increases to

$$L_E = L - \frac{B}{\pi}\left[\ln\left(\frac{\pi B}{\lambda}\right) + \Gamma - 3/2\right], \tag{5}$$

and thus the total 'mass' of the oscillator increases (previously given by the amount of water within the strait). Here $\Gamma = 0.5772..$ denotes Euler's constant. This leads to a corresponding decrease of the Helmholtz frequency (see (7) below). Second, this radiation damping gives rise to an additional damping term, linear in this case, which will simply be added below.

We non-dimensionalize as follows: $z_* = Hz$, $\zeta_i = H\zeta$, $A_*(z_*/H) = A_0 A(z)$, $V_* = A_0 HV$, with dimensionless excess volume

$$V \equiv \int_0^{\zeta} A(z)\mathrm{d}z, \tag{6}$$

$\zeta_e = HZ_e$ and $t_* = t/\sigma_H$, where the square of the Helmholtz frequency, σ_H, is defined as

$$\sigma_H^2 = gHB/A_0 L. \tag{7}$$

Employing these scales in (3) and (4), eliminating u, and incorporating the linear damping term, leads to the equation for the Helmholtz resonator in terms of the excess volume $V(t)$:

$$\frac{\mathrm{d}^2 V}{\mathrm{d}t^2} + \zeta(V) = Z_e(\sigma t) - r\frac{\mathrm{d}V}{\mathrm{d}t} - \gamma\left|\frac{\mathrm{d}V}{\mathrm{d}t}\right|\frac{\mathrm{d}V}{\mathrm{d}t}. \tag{8}$$

Here $r = \sigma B/2L$ is the radiation damping coefficient, and $\gamma = (\delta/L + k/H)A_0/B$ is the aggregate of quadratic damping coefficients. The restoring term, the second term on the left, is considered to be a function of the excess volume determined by the actual shape of the basin. Its dependence $\zeta(V)$ will be discussed below for a constant- and variable-depth basin respectively. Forcing by the external tide is assumed to be

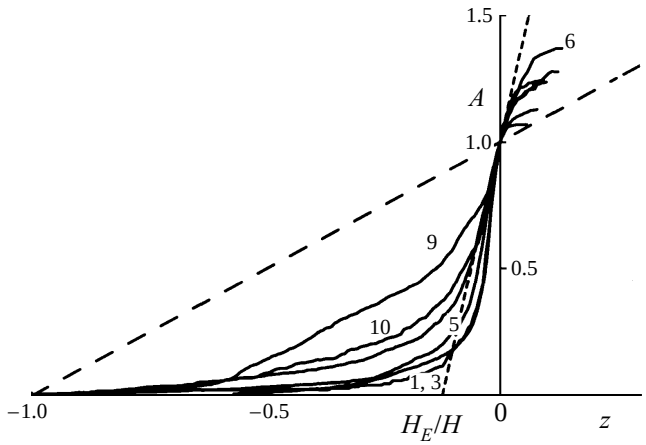

FIGURE 3. Hypsometric curves (giving surface area, $A(z) = A_*(z)/A_0$ as a function of height $z = z_*/H$) for some Wadden Sea basins whose numbers refer to figure 1 and table 1. The long-dashed line gives the linear area–height relationship employing maximum depth of each basin. The short-dashed line is a linear area–height relationship for the Zoutkamperlaag basin (#6) approximating the true hypsometric curve closely near mean sea level. Its intercept with the z-axis gives the (dimensionless) *effective* depth H_E, which is about 12% of the true maximum depth H given in table 1.

sinusoidal

$$Z_e = F \cos \sigma t, \tag{9}$$

and is characterized by its amplitude F and scaled tidal frequency $\sigma = \sigma_e/\sigma_H$. The forcing parameters, together with damping parameters r and γ, will be treated as independent quantities, and the effect of different choices will be considered.

3. Helmholtz resonator in a basin of constant depth

When the depth within the basin is uniform, the area $A(z) = 1$ and thus, from (6) , $V = \zeta$. Hence, in this case, the restoring term in (8) is linear. In the absence of quadratic damping it reduces to the familiar equation describing a forced and damped linear oscillator, which is able to resonate for weak enough damping.

With the nonlinear damping term included this reduces to an equation proposed by van der Kreeke (1988) and DiLorenzo (1988). The nonlinearity generates higher harmonics (Mehta & Özsoy 1978, and references therein), which in turn may resonate at the Helmholtz frequency. Out-of-resonance damping is controlled by radiative processes, for which the response is proportional to the forcing amplitude F, while, near resonance, it is controlled by frictional processes, for which the response is proportional to $F^{1/2}$ (Zimmerman 1992).

4. Helmholtz resonator in a basin of variable depth

More often than not the sides of a basin slope (Boon & Byrne 1981). This is prominently visible in figure 3, which gives hypsometric curves (area A as a function of height z) of some of the Wadden Sea tidal basins (see table 1). The Wadden Sea basins show a moderate degree of tidal amplification. Although at high tides there is some basin-to-basin mass flux over the watersheds this does not exceed a few percent of the tidal prism (Ridderinkhof 1988). Consequently, it is assumed here that these

# in figure 1	Basin name	A_0 km^2	H m	H_E m	L km	L_E km	B km	σ_H 10^{-4} s^{-1}	σ
1	Marsdiep	755	38	4	6	9.0	2	1.1	1.3
2	Eierlandse gat	157	9.3	1.6	4	6.7	2	1.7	0.8
3	Vlie	650	20	2.7	5	8.9	3	1.2	1.2
4	Borndiep	274	20	2	4	6.8	2	1.5	1.0
5	Wierumerwad	52	10	1.4	2	5.6	3	3.8	0.4
6	Zoutkamperlaag	107	15	1.9	3	6.8	3	2.8	0.5
7	Eilanderbalg	46	16	1.3	1	3.1	1.5	3.7	0.4
8	Lauwers	116	20	1.7	2	4.7	2	2.5	0.6
9	Schild	32	3.5	1.7	1	2.6	1	4.5	0.3
10	Eems	375	25	4.2	3	8.2	4	2.3	0.6
11	Dollard	54	11	1.9	6	9.8	3	3.3	0.4
12	Westerbalgje	263	23	2.4	3	7.8	4	2.2	0.6

TABLE 1. Identification of tidal basins in Dutch Wadden Sea, enumerated in figure 1, with several characteristic parameters: the basin's mean surface area A_0, maximum depth H, effective depth H_E (determined in a manner as explained in figure 3 for the Zoutkamperlaag basin), and length L and width B of the connecting strait. From these the Helmholtz frequency σ_H (based on effective depth H_E and length L_E, equation (5)) and non-dimensional forcing frequency $\sigma = \sigma_e/\sigma_H$ are obtained.

basins can be treated as if they were isolated. Further work on connected basins is needed to assess the validity of this assumption, which will also be relevant to unambiguous multiple-inlet basins.

Previous formulations for Helmholtz resonators in basins with variable depth have either treated the change in surface area with height parametrically (van de Kreeke 1988; DiLorenzo 1988), or have focused on the spatial dependence of the basin's response, disregarding the nonlinearity which this implies for the basin–strait system as a whole (Miles & Lee 1975). To go beyond the simple constant-area (constant-depth) basin, Green (1992) assumed a linear dependence on height

$$A(z) = 1 + z, \tag{10}$$

the offset being due to the fact that the deepest point of the basin is non-dimensionally at $z = -1$, while, in view of the adopted non-dimensionalization, $A(0) = 1$. Comparison with figure 3 shows that such a model is more applicable when true depth is replaced by a (shallower) effective depth for which the linear relationship (10) holds better. It is this effective depth which then determines the Helmholtz frequency (7). With this linear expression (10) the excess volume elevation relationship is, from (6),

$$V = \zeta + \zeta^2/2. \tag{11}$$

Since $\zeta = 0$ when $V = 0$ this yields, inversely, the nonlinear restoring term

$$\zeta(V) = (1 + 2V)^{1/2} - 1. \tag{12}$$

Notice that (12) implies that the basin is 'non-empty' as long as $V > -1/2$. (The non-dimensional volume of the unforced basin at rest equals $1/2$). The evolution equation of the excess volume (8), together with the restoring term (12), constitutes the nonlinear oscillator which describes the response of a basin whose area decreases linearly with depth, and which is connected to an open sea by a narrow strait, due to a (tidal) wave at the entrance of frequency σ and shape determined by $Z_e(\sigma t)$). Note that $\mathrm{d}V/\mathrm{d}t$ is, by (4), physically related to the current strength in the strait. Although emphasis here is on the response of almost-enclosed basins to tides it is clear

that the same approximation applies to the response to waves at any other forcing frequency, such as that of harbours to tsunamis (Miles 1974) and swell (Okihiro, Guza & Seymour 1993), or that of coupled lakes to storms (Sorensen & Seelig 1976).

Green (1992) addressed (8) and (12) in the free, inviscid and unforced case in the small-amplitude limit, in which case the rescaling $\zeta = \epsilon\eta$, with $\epsilon \ll 1$ a small parameter, leads to a nonlinear equation for η, which he subsequently studied using the Lindstedt–Poincaré method (Nayfeh 1973). This method solves a nonlinear (oscillator) equation by assuming a perturbation expansion not only for the amplitude, but also for the frequency. He showed that higher harmonics are generated at $O(\epsilon)$, while the frequency increases with $O(\epsilon^2)$. It turns out that this free response need not necessarily be studied perturbatively as it can be obtained in closed form.

4.1. *Exact free response*

The free ($F = r = \gamma = 0$), nonlinear Helmholtz response of a basin with linear variation of area with depth (10) is thus, from (8) and (12), governed by

$$\frac{\mathrm{d}^2 V}{\mathrm{d}t^2} + (1 + 2V)^{1/2} - 1 = 0. \tag{13}$$

Note that the second and third terms above together constitute the restoring term, and the last, constant term should thus not be regarded as 'forcing'. Also note that this equation reduces to the harmonic oscillator for infinitesimal amplitudes of the excess-volume fluctuations. This equation is most easily solved by writing it in terms of the occupied area at surface level $A \equiv A(\zeta) = 1 + \zeta$ to which the excess volume is, according to (6), related by

$$V = (A^2 - 1)/2. \tag{14}$$

With this substitution we find that surface area A is governed by

$$\frac{\mathrm{d}}{\mathrm{d}t}\left(A\frac{\mathrm{d}A}{\mathrm{d}t}\right) + A - 1 = 0. \tag{15}$$

This is the same equation that also governs the shape of long, nonlinear waves, subject to Coriolis dispersion, in a co-moving frame of reference – see Ostrovskiy (1978), who discusses phase-plane trajectories of this equation. Multiplying (15) with $A\mathrm{d}A/\mathrm{d}t$, and integrating once, we obtain

$$\frac{1}{2}\left(A\frac{\mathrm{d}A}{\mathrm{d}t}\right)^2 = q + A^2/2 - A^3/3 \equiv P_3(A) = (a - A)(A - b)(A - c)/3, \tag{16}$$

where q is an integration constant, related to an 'energy-level', which is determined by the initial area and rate of change. The right-hand side of this equation is a third-degree polynomial $P_3(A)$ that needs to be positive and hence its factorization requires $b < A < a$, see figure 4(a). Its solution $A(t)$ can be obtained parametrically as

$$A(\tau) = a - (a - b)\mathrm{sn}^2(\tau|m), \tag{17}$$

$$t(\tau) = \left(\frac{6}{a - c}\right)^{1/2}[c\tau + (a - c)E(\tau|m)], \tag{18}$$

with $\mathrm{sn}(\tau|m)$ the Jacobian elliptic function and $E(\tau|m)$ the elliptic integral of the second kind (Abramowitz & Stegun 1964). The zeros of $P_3(A)$ are given by $a, b, c = 1/2 + \sin\alpha_{1,0,-1}$, where $\alpha_k = (2\pi k - \beta)/3$, while parameter $m = (a - b)/(a - c)$. Here auxiliary variable $\beta = \sin^{-1}(1+12q)$, which leads to real zeros provided $-1/6 \leqslant q \leqslant 0$.

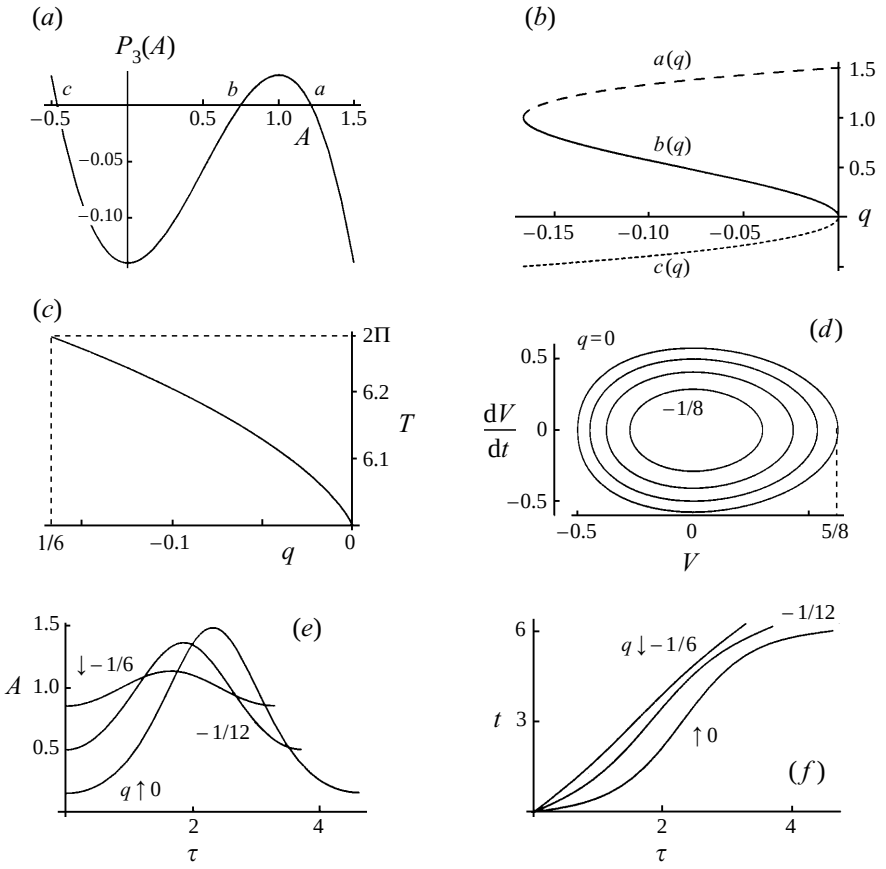

FIGURE 4. Analytic solutions of free mode: (*a*) $P_3(A)$ for $q = -0.14$ in which roots a, b and c are identified. (*b*) Roots a, b, c of $P_3(A) = 0$ as functions of q. (*c*) Period $T(q)$. (*d*) Isolines in phase space, for $q = 0, -1/24, -1/12, -1/8$. (*e*) Parametric solution curve $A(\tau)$, and (*f*) $t(\tau)$, for $q \downarrow -1/6$, $q = -1/12$ and $q \uparrow 0$.

Since $\mathrm{sn}^2(\tau|m)$ is $2K$-periodic and $E(\tau + 2K|m) = E(\tau|m) + 2E$ (with $K \equiv K(m)$ and $E \equiv E(m)$, the complete elliptic integrals of the first and second kind respectively), from (18), the period of this solution, T, can also be obtained:

$$T = 2\left(\frac{6}{a-c}\right)^{1/2}[cK + (a-c)E]. \tag{19}$$

Equations (14), (17) and (18) together form the parametric solution of (13) and some graphs may serve to illustrate it.

Figure 4(*a*) displays polynomial $P_3(A)$ for a particular value of q and identifies the three roots of the cubic, displayed in figure 4(*b*) as a function of q. For $q \downarrow -1/6$, b and a are close to, but on either side of 1, the infinitesimal distance $a-1$ representing the amplitude of the sea surface oscillation. The solution in this case is sinusoidal, oscillating between these two extreme values. For $q = 0$, $b = c$ and the sea level becomes a set of 'coupled parabolas': $\zeta = 1/2 - t^2/6$, with $t \in [-3, 3)$, (mod 6). The basin just empties at low tide. (Curiously, the quadratic time-dependence of the surface elevation in this fully nonlinear case seems to imply that (except at low tide) the gravitional acceleration which particles residing at the surface experience

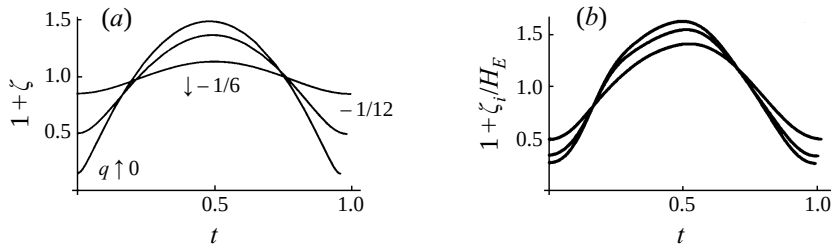

FIGURE 5. (*a*) Free response of the surface area $A = 1 + \zeta$, related to the excess volume by $V = (A^2 - 1)/2$, as given by the parametric solutions of the unforced and inviscid evolution equation for V, for initial conditions varying from linear ($q \downarrow -1/6$) to fully nonlinear ($q \uparrow 0$). Time is scaled with the period of a linear wave: 2π. (*b*) Average spring, mean and neap tidal elevation over one tidal period (T), as observed by Rijkswaterstaat in Lauwersoog at the end of Zoutkamperlaag basin (#6) in the Dutch Wadden Sea. Displayed is $1 + \zeta_i/H_E$, a scaled and off-set version of the observed elevations, so as to be comparable with the free-mode. Equivalent depth has, in accordance with the observation in figure 3, been taken as 12% of maximum depth, $H_E = 1.9$ m. Time is scaled with the lunar, semi-diurnal tidal period.

is less than g, as gravity g is now reduced by the uniform acceleration $\mathrm{d}^2\zeta/\mathrm{d}t^2$, dimensionally equalling $-H\sigma_H^2/3 = -gH^2B/3A_0L$.) Although the asymptotic form of the free surface can be obtained from the general solution (17) and (18) in the limit $q \uparrow 0$ it is most easily obtained by directly integrating (16) with $q = 0$.

In figure 4(*c*), the period of the oscillation T is shown as a function of q. It has a slight variation decreasing from 2π in the linear limit ($q \downarrow -1/6$) to 6 in the fully nonlinear limit ($q \uparrow 0$). (In the latter case, with the asymptotic parabolic shape just discussed, $A = 1 + \zeta$ vanishes at $t = \pm 3$, which confirms that the period $T = 6$.) A useful representation of the solution can be given in the 'phase-space' spanned by $\mathrm{d}V/\mathrm{d}t$ and V, where, for each value of integration constant q, time acts as a parameter tracing out a certain solution curve (see figure 4(*d*)). It should be noted that the outermost curve (corresponding to $q = 0$) bounds the part of phase space that has stable solutions. Initial values outside this curve should be avoided as isolines cross the $V = -1/2$ line at which the restoring term (12) becomes meaningless. This same phenomenon, namely the presence of a bounded region in phase space over which stable solutions exists, also occurs in the forced and damped cases, considered below, although the extent of this stable domain has not been further assessed in this study. Figure 4(*e*, *f*) gives the dependence of surface area A (displaced sea level) and time t on parameter τ. These two graphs can be combined to give the actual evolution $A(t)$, as in figure 5(*a*), showing the cusped structure in the fully nonlinear case characterized by long-lasting highs and short lows.

4.1.1. *Hamiltonian structure*

Integration constant q was given the physical meaning of representing an 'energy-level'. This can be seen by writing (13) in Hamiltonian form

$$\frac{\mathrm{d}V}{\mathrm{d}t} = y \equiv \frac{\partial H}{\partial y}, \tag{20}$$

$$\frac{\mathrm{d}y}{\mathrm{d}t} = 1 - (1 + 2V)^{1/2} \equiv -\frac{\partial H}{\partial V}, \tag{21}$$

which implies a Hamiltonian

$$H(V, y) = \tfrac{1}{2}\left(y^2 - (1 + 2V) + \tfrac{2}{3}(1 + 2V)^{3/2}\right), \tag{22}$$

where a constant has been slipped in for convenience. Because of (14), H can formally also be written as

$$H = \tfrac{1}{2}(y^2 - A^2 + \tfrac{2}{3}A^3), \tag{23}$$

which shows, from (14), (16) and (20), that on fixed energy levels, $H = constant$, we may identify $q = H$. A Hamiltonian form can likewise be obtained in the forced case, with a non-zero time-dependent right-hand side $Z_e(t)$, by simply adding a term $-VZ_e(t)$ to (22) and (23). The Hamiltonian structure of the unforced equation guarantees the existence of closed 'tori' (curves in this unforced one degree-of-freedom case), while a weak perturbative forcing can be anticipated to lead to the formation of weak chaos (Zaslavsky *et al.* 1991). This will be discussed later on.

4.1.2. *Comparison of observed tide and free mode*

As table 1 shows, most Wadden Sea basins are close to resonance with the semi-diurnal tide. This in itself is a striking result. It not only makes it plausible that some of the processes discussed here might be of relevance to such tidal basins, but carries the suggestion that the dimensions of the basin are not a coincidence, but are themselves shaped by the presence of a resonance. They might reflect a kind of 'most unstable mode' of the sedimentary environment.

Figure 5(*b*) gives the average observed tidal elevation at neap, mean and spring tide in basin 6 of figure 1 (Zoutkamperlaag). Like the free solution, figure 5(*a*), it shows, with increasing amplitude, both a change in tidal profile from sinusoidal to parabolic, and a shortening of the 'duration of the tidal period'. From the analogy with a similar decrease in period for the free response (figures 4*c* and 5*a*) this observed decrease might therefore perhaps be related to the nonlinear response of the tidal basin to a single-frequency semi-diurnal (M_2) forcing. However, we have to acknowledge that such an amplitude-dependent change in period of a nonlinear oscillator is a property of an inviscid dynamical system only (see §4.2). In contrast, when viscous effects are present, apart from transient oscillations, such modulation is absent (see §4.3). It is more likely therefore that this change may simply be explained by the linear superposition with a second semi-diurnal forcing frequency component of solar origin (S_2), which, coincidently, leads to a similar shortening (lengthening) of the tidal duration at spring (neap) tide. At present therefore it is unclear to what extent nonlinearity amplifies this linear effect in nature.

The rather pronounced change in tidal profile (reflected in an increasing amount of higher harmonics) for increasing 'tidal range' while going from neap to spring tide lends some support to the suggestion that the tide within the basin is determined by the dramatically shallower, *effective* depth (whose determination has been sketched in figure 3) rather than by true, maximum depth. This is also suggested by the strong bias towards shallower depths which hypsometric curves in this figure demonstrate. For this reason effective depth has been employed to scale the observed tide in figure 5(*b*), as well as in the determination of the Helmholtz frequency in table 1. It shows that tidal basins might be 'more nonlinear' than is anticipated on the basis of a basin's maximum depth.

Although the similarity between figures 5(*a*) and 5(*b*) suggests that the response of the forced and damped nonlinear oscillator is perhaps dominated by the free response, in reality tidal forcing and friction cannot be neglected. For this reason these processes are subsequently added in what follows.

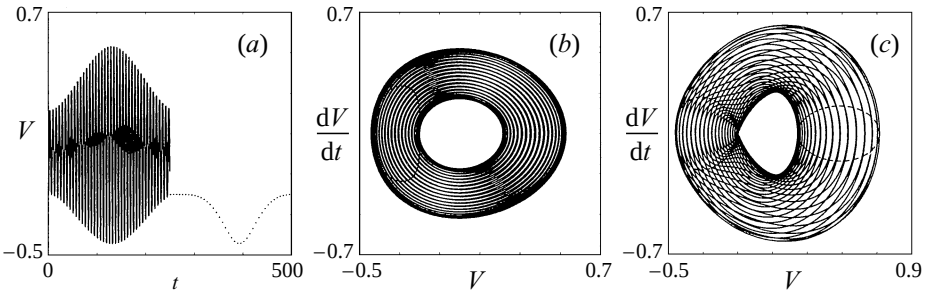

FIGURE 6. (*a*) Numerical integration of the inviscid, forced evolution equation (24) for the excess volume V and sinusoidal forcing (9) (solid curve), demonstrating resonant growth, natural detuning and subsequent decay for $F = 0.01$ and $\sigma = 1$, as given by V versus time t for $V(0) = -0.2$, $\mathrm{d}V/\mathrm{d}t(0) = 0$. Integration extends to $t = 250$. The dotted curve gives a stroboscopic plot at $\sigma t = (2n + 1)\pi$, with n an integer, up to $t = 500$. (*b*) Phase-space trajectory of this solution, $\mathrm{d}V/\mathrm{d}t$ versus V, and, superimposed (curve on the left) Poincaré (stroboscopic) plot, see (*a*). (*c*) Same as (*b*) for $F = 0.2$ and $\sigma = 2$, starting at initial point $V(0) = -0.1$, $\mathrm{d}V/\mathrm{d}t(0) = 0$.

4.2. *Inviscid response to forcing*

Although the consideration of the forced inviscid equation (see (8), with $r = \gamma = 0$),

$$\frac{\mathrm{d}^2V}{\mathrm{d}t^2} + (1 + 2V)^{1/2} - 1 = Z_e(t), \tag{24}$$

with $Z_e(t)$ the external tide, is perhaps without much physical interest there are some mathematical aspects of it which justify it being considered briefly. First, a forced nonlinear equation, unlike its linear counterpart, is not necessarily singular when forced at resonance. This is due to the natural detuning (amplitude-dependent shift of resonance frequency) accompanying the growth of the response. Second, a forced nonlinear oscillator is of general interest because of the possibility of chaos that such a system constitutes. To delineate if and under what circumstances this occurs is one of the prime goals in dynamical system research. Third, the particular form of the nonlinear restoring term addressed here is of some interest because it exhibits some features not found in classical nonlinear oscillators, like the pendulum, and van der Pol and Duffing oscillators.

4.2.1. *Amplitude modulation*

For fixed forcing (frequency and amplitude of the external tide), the amplitude of the tidal oscillation within the basin may vary on a long time scale when the forcing frequency is near resonance. This can be explained as follows. Tidal levels are increasing due to the near resonance of the basin. However, the eigen-frequency of the basin is now a function of the amplitude (see figure 4*c*) and thus will change (natural detuning). As a consequence, the system is brought out of resonance and the tidal amplitude drops, from which point the cycle starts again (see figure 6*a*). In figure 6*b* this solution is presented in phase space. It shows that due to the weak forcing the phase-space trajectory drifts from orbit to orbit approximately retracing its steps in a quasi-periodic way. In that same figure a 'stroboscopic' version of the trajectory – a Poincaré plot – has also been presented, which gives the basin's volume at times when the external tide is low (at a minimum). It displays the regular character of the modulation and the quasi-periodicity by the fact that it is a continuous line. Similar features arise for other frequencies, as e.g. seen in figure 6(*c*) for forcing at twice the (linear) Helmholtz frequency, $\sigma = 2$. (Notice that this implies that the forcing

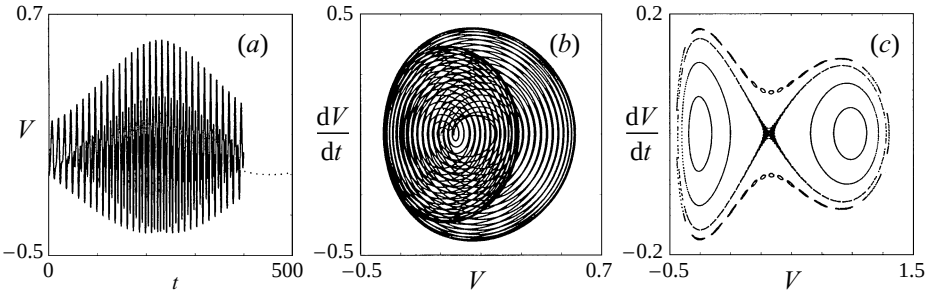

FIGURE 7. (*a*) Numerical integration of the inviscid ($r = \gamma = 0$) forced evolution equation (24) for the excess volume V, forced by (9) for $F = 0.1$ and $\sigma = 1/2$, as given by V versus time t for $V(0) = -0.1$, $\mathrm{d}V/\mathrm{d}t(0) = 0$. (*b*) Phase-space trajectory of this solution, $\mathrm{d}V/\mathrm{d}t$ versus V. (*c*) Poincaré plot in phase space, $\mathrm{d}V/\mathrm{d}t$ versus V, for $F = 0.785$ and $\sigma = 1.917$, of four orbits in which 'traces of chaos' are evident in the erratic central orbit. Note that the two inner 'orbits' consist of a left and right segment each.

has period π, while the free response has period $6 \leqslant T \leqslant 2\pi$. Therefore the free response is dominated by the *subharmonic* and a stroboscopic picture of this with the forcing period alternately gives points roughly below and above mean sea level, see also figure 7*c*.) Forcing frequencies below the Helmholtz frequency (figure 7*a*) have phase-space trajectories (figure 7*b*) that traverse two different level sets. Poincaré plots, nevertheless, in general trace out regular curves. One exception to this statement is seen in figure 7(*c*) to be discussed now.

4.2.2. *'Chaotic tides'*

Interest in forced nonlinear oscillators, like the forced pendulum, or van der Pol or Duffing oscillators, is fuelled by the possible existence of chaos (Rasband 1989; Parker & Chua 1989). Chaos in these equations occurs for weak forcing because of destruction of separatrices in the unforced system, which connect saddle points with themselves (homoclinic), or with each other (heteroclinic connections). The onset of chaos ('stochasticity') is attributed by Zaslavsky *et al.* (1991) to the fact that the period of the unforced orbits increases from a finite value at a centre to infinity at the separatrix. The effect of weak forcing on the free response will be weak near the centre but large near the separatrix, because the period will be changed only slightly in the former but dramatically in the latter case. Consequently, the phase of the particle within a period of its orbit (related to its location in phase space when observed at regular time intervals) also changes only little near the centre, but wildly near the separatrix. Interestingly, however, the forced inviscid version of (8),

$$\frac{\mathrm{d}V}{\mathrm{d}t} = y, \tag{25}$$

$$\frac{\mathrm{d}y}{\mathrm{d}t} = 1 - (1 + 2V)^{1/2} + Z_e(t), \tag{26}$$

has, for vanishing forcing, only one critical point, which is a centre. Moreover, the period of the orbits never increases to infinity, but rather decreases slightly, from 2π to 6. The standard ingredients for the occurrence of chaos are thus not available. In passing it should be remarked that an even-ordered truncation of a Taylor expansion of the nonlinear restoring term may obscure this result as it apparently always has two real zeros, one of which is a saddle which does have an infinite-period self-

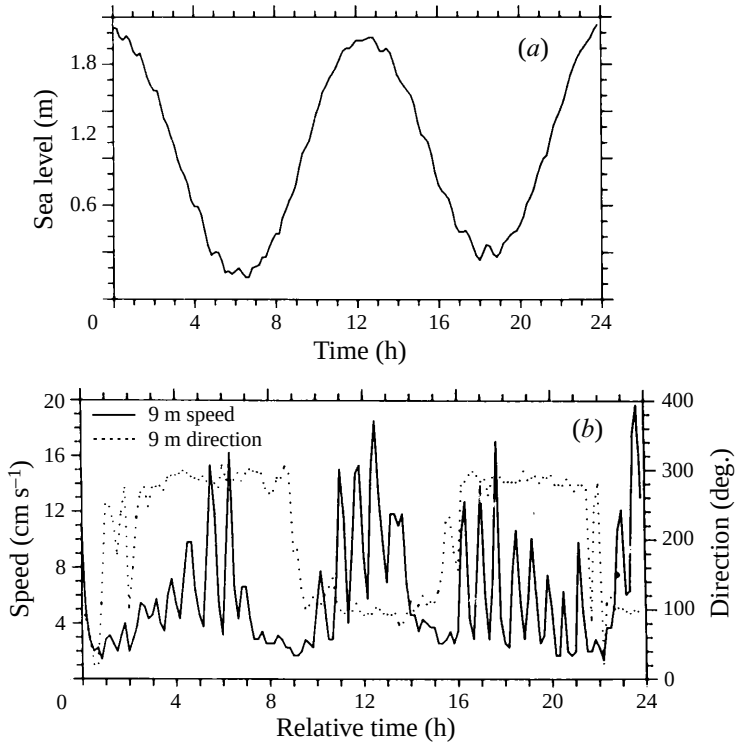

FIGURE 8. Irregular observed sea level (*a*) and current (*b*) observations versus time in Moldefjord, Norway (from Golmen *et al.* 1994).

intersecting separatrix that may, by destruction, suggest the occurrence of chaos, despite its absence in the exact form of the nonlinear restoring term.

Although a saddle point, the classical ingredient for chaos, may be absent, there nevertheless seems to exist a tiny region in parameter space for which numerical calculations of the nonlinear Helmholtz oscillator (with the exact restoring term), subject to sinusoidal forcing (9), suggest the solutions to be chaotic (see figure 7*c*). It is speculated that this is because of the occurrence of a saddle point in the Poincaré map. The period of the modulation in this case goes to infinity at the separatrix and it is the sensitiveness to the change in modulation period in the neighbourhood of this separatrix which creates the big changes in phase that might lead to a chaotic response. This leads to the counterintuitive but intriguing suggestion that one may occasionally expect to observe 'chaotic tides', an expression that, in view of the extreme regularity of the tidal forces, might at first look be thought a contradiction in terms!

4.2.3. *Field observation of irregular tides*

That tides in almost-enclosed basins can be chaotic is suggested by the observations of Golmen, Molvaer & Magnusson (1994), see figure 8, who, in a fjord in Norway, observed an 'irregular' sea level and, in particular, current modulations of about 45 minutes period, whose origin they, in view of the persistency of this phenomenon, attribute to the tides. To what extent the 'chaos' in their tidal observations can be explained by the above (inviscid!) mechanism, however, is as yet unclear, in particular as the chaos in the theoretical model does not seem to persist under the addition of

friction. Further analysis is also needed of this case, for which the forcing period is much larger than the free period, $\sigma \ll 1$.

4.3. *Viscous response to forcing: multiple steady states*

If, more realistically, we do include friction, direct integration of (8) indicates that the system generally settles down into a steady state (a response curve, $V(t)$, of particular amplitude $\hat{V}$, phase and shape), which is usually independent of initial conditions. The temporal shape of these steady states may include (but can also be more complex than) the free mode given in figure 5(*a*). It may for instance exhibit an intermediate minimum/maximum within one period, while it may also feature asymmetric profiles, of relevance for net sediment transport. However, the amplitude response curve – giving the amplitude of a steady state as a function of forcing frequency – need not always indicate that there is a unique state: systems close to resonance may exhibit *multiple equilibria.*

4.3.1. *Approximate stationary response in the small-amplitude limit*

When the excess-volume fluctuations $V(t)$ are of small amplitude (and when the forcing and frictional parameters are also small) (8) can be approximated by rescaling $V \to \epsilon V$, $r \to \epsilon^2 r$, $\gamma \to \epsilon^2 \gamma$, $F \to \epsilon^3 F$ (with $\epsilon \ll 1$). The choice for this particular ordering of parameters is motivated by our desire to obtain a uniformly valid approximate solution of (8) and (12) in which damping, forcing and nonlinearity all appear at the same order in our perturbation scheme (Nayfeh & Mook 1979). With (9), this scaling leads to the following equation:

$$\frac{\mathrm{d}^2 V}{\mathrm{d}t^2} + V = \frac{\epsilon}{2} V^2 - \frac{\epsilon^2}{2} V^3 + \epsilon^2 F \cos(\sigma t) - r\epsilon^2 \frac{\mathrm{d}V}{\mathrm{d}t} - \gamma \epsilon^2 \left| \frac{\mathrm{d}V}{\mathrm{d}t} \right| \frac{\mathrm{d}V}{\mathrm{d}t} + O(\epsilon^3). \tag{27}$$

This can be considered an extension of Green's (1992) small-amplitude equation to which forcing and damping terms have been added. Note that the odd-ordered Taylor series truncation guarantees that the restoring term has only one real zero. This equation is, following the derivation in Nayfeh & Mook (1979, p. 196), solved by a multiple-scale perturbation expansion and has an amplified response at $\sigma = 1, 1/2, 1/3, 2/3, .., 2, 3, .., 3/2, ...$ The nonlinear friction term is expanded in its Fourier series and, by requiring the absence of secular terms in the equations governing the subsequent orders of the perturbation expansion, near the primary resonance (which, for consistency, requires $\sigma = 1 + \epsilon^2 \omega$) the following result is obtained. The solution is, up to second order, given by

$$V = \hat{V} \cos(\sigma t - \phi) + \tfrac{1}{4} \epsilon \hat{V}^2 [1 - \tfrac{1}{3} \cos 2(\sigma t - \phi)] + O(\epsilon^2). \tag{28}$$

The response is thus frequency-locked to the forcing. Also it exhibits a 'drift' term (the constant term) providing a net displacement of the mean state. Here the amplitude $\hat{V}$ and phase ϕ vary on a slow time scale governed by

$$\hat{V}' = -\frac{r}{2} \hat{V} - \frac{4\gamma}{3\pi} \hat{V}^2 + \frac{F}{2} \sin \phi, \tag{29}$$

and

$$\hat{V} \phi' = \omega \hat{V} - \frac{1}{12} \hat{V}^3 + \frac{F}{2} \cos \phi, \tag{30}$$

where a prime indicates differentiation with respect to the slow time variable $\epsilon^2 t$. Of particular relevance are the steady states of these latter equations to which all solutions tend during the decay from the particular initial conditions they start

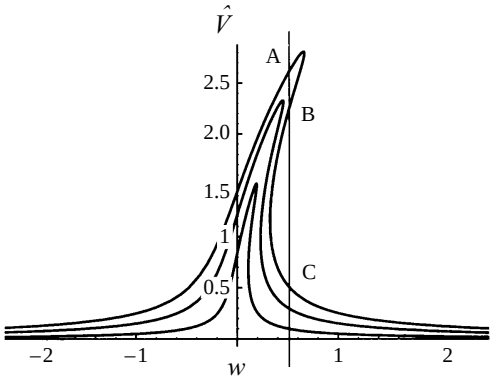

FIGURE 9. Amplitude response $\hat{V}$-curves against detuned frequency $\omega \equiv (\sigma - 1)/\epsilon^2$ (with $\epsilon \ll 1$ the detuning parameter). For cases of near-resonant forcing, $\sigma \approx 1$, it has bent 'resonance horns' indicating multiple equilibria and an increased response when F increases from 0.1 to 0.3 and 0.5, for frictional parameters $r = \gamma = 0.01$. Near $\omega \approx 0.5$ three equilibria, A, B and C, are obtained where the vertical line intersects the amplitude-response curve (for $F = 0.5$). The smallest and largest of these intersections are stable and correspond to a choked (C) and amplified (A) regime respectively.

with. These are obtained by equating the right-hand sides to zero, which yields the frequency-response curve

$$\omega = \frac{1}{12}\hat{V}^2 \pm \frac{1}{2}\left\{\left(\frac{F}{\hat{V}}\right)^2 - \left(r + \frac{8\gamma}{3\pi}\hat{V}\right)^2\right\}^{1/2}, \tag{31}$$

see figure 9. This figure shows for some particular values of forcing and friction parameters, that, near resonance, bended resonance horns occur. For these parameter values this indicates the presence of three equilibria, two of which (A and C) are stable and one (B) unstable. This simultaneous presence of an amplified regime A ($\hat{V} > 1$) and a choked regime C ($\hat{V} < 1$), for the same parameter values, most compactly presents the opposing tendencies to which a tidal basin, connected to the open sea by a narrow channel, is subject.

In a similar way the response can be determined for forcing frequencies which are, for instance, near twice or half the Helmholtz frequency. They yield a combined harmonic and subharmonic or superharmonic response respectively.

4.3.2. *Multiple steady states in the exact model*

Results in the previous section may be quantitative, but are obtained for a polynomial approximation of the exact algebraic restoring term (12). Since, near resonance, the amplitude of the response may be amplified this casts doubt on the correctness of omitting higher-order terms and it leaves one wondering whether the existence of multiple steady states holds also with the full nonlinear restoring term (12) present. For this reason a numerical integration of (8) with parameter values as suggested by those from the previous section has been performed with the dynamical systems tool DSTOOL (Guckenheimer *et al.* 1992) employing a fourth-order Runge–Kutta integrator. The Poincaré plot of this is seen in figure 10(*a*), which confirms that multiple steady states (the centres of the two stable foci) may exist simultaneously, but now at finite amplitudes of the basin's excess volume V and channel flow $\mathrm{d}V/\mathrm{d}t$. The presence of fixed points in the Poincaré map also confirms that the response is locked

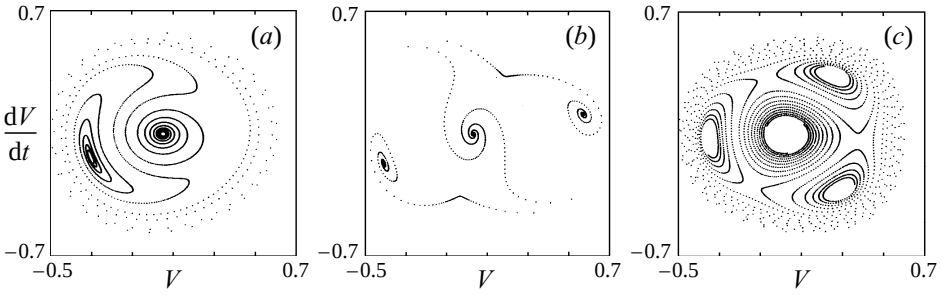

FIGURE 10. (*a*) Poincaré plot of numerical integration of (8) for $\sigma = 1.01$, $F = 0.001$, $r = 0.001$ and $\gamma = 0$, for various initial conditions, indicating the presence of two stable foci. (*b*) Same as (*a*) for $\sigma = 2.04$, $F = 0.1$, $r = 0.01$ and $\gamma = 0$. There are two steady states to which trajectories in phase space tend. The central, small-amplitude one has forcing period. The large-amplitude one is a subharmonic and its period is twice that of the forcing and thus shows up as a *pair* of points in the Poincaré plot (the two off-centre points to which the spirals tend). (*c*) Same as (*b*) for $\sigma = 3.04$, $F = 0.2$, $r = 0.001$ and $\gamma = 0$, but the large-amplitude steady state now has period three times that of the forcing.

to the forcing, as in the small-amplitude approximation. Note in this figure also that a finite-amplitude response is obtained despite the weakness of the forcing. It remains to be seen whether this result can be extended to larger values of forcing and friction such that the amplification reaches values obtained in nature. Multiple steady states are also obtained for forcing frequencies a little above 2 and 3 (see figure 10*b*, *c*), except that the small-amplitude (central) state is dominated by a response at the forcing frequency, while the large-amplitude state is dominated by the subharmonic (which is near the frequency of the free mode). This manifests itself in the Poincaré map as fixed points of period 2 and 3 respectively. No amplitude-response curves for the exact fully nonlinear restoring term have been obtained so far.

4.3.3. *Field indications of changing tidal ranges*

The bent resonance horn in figure 9 and the Poincaré plots of figure 10 indicate that, for the same values of the 'parameters of the system' (characterizing forcing and friction), the basin may respond with either a small- or large-amplitude oscillation. These states have their own 'basins of attraction' that do depend on initial conditions (Nayfeh & Mook 1979) and may, in fact, do so in a fractal manner, as a study on the forced and damped pendulum has shown (Grebogi *et al.* 1990). The implication of the bend in the resonance horn is that one of these modes may cease to exist for 'quasi-stationary' changes of the parameter values, when the frequency band over which multiple equilibria exist is left. Thus, when this happens, the system may have to change its behaviour rapidly to the only remaining state, thereby shifting to a tidal regime with smaller or larger range. Changes like these may perhaps be triggered by changes in mean sea-level, which, in view of the adopted scaling, translates into a change of F in (31). With reference to observations in the Strangford Lough, Northern Ireland, it has been suggested by Dr G. Savidge of the Queen's University of Belfast (personal communication) that evidence of such rapid changes in tidal amplitudes of almost-enclosed basins may be hidden in observed sedimentological zonation patterns. An abrupt drop in tidal amplitude may ultimately form the most dramatic demonstration that a tidal basin with sloping bottom constitutes a nonlinear Helmholtz resonator.

5. Summary and discussion

Closed basins possess eigenmodes which are characterized by the trivial fact that they conserve the enclosed fluid volume. These modes differ only slightly when the basin communicates with an open sea through a narrow strait. However, one additional mode appears, which does break the above constraint. This is the pumping, or Helmholtz mode, characterized by a periodic mass (volume) exchange with the open sea. This low-frequency mode is generally also the most energetic mode present. This mode is characterized by the absence of a spatial dependency of the sea surface elevation within the basin, and can thus be described simply by one time-dependent parameter: the excess volume (which gives, at any moment, the excess amount of fluid when compared with the undisturbed fluid volume). The volume, and related sea-level, change due to the transport of water through the connecting strait. This transport of water is, in turn, driven by the pressure difference, due to a difference in sea-level heights which exists between the entrance and exit of this channel. The sea level of the open sea is determined mainly by the tide and is thus a prescribed function of time. The sea level in the basin is determined by the volume flux through the strait and by the change which this is consequently able to produce, radiative and frictional effects being accounted for by linear and quadratic damping terms and by a change in the effective length of the strait. For a basin with vertical sidewalls this sea-level change is linearly proportional to a change in fluid volume. When the basin has sloping sidewalls (increasing surface area with increasing height), however, the amount of sea-level change which a given volume flux produces in a certain period of time depends on the pre-existent water level. When this level is low the change will be large, as the surface area occupied is small. Conversely, when the initial basin sea level is high its change will be small, as the occupied surface area is large. The sea level within the basin thus is a nonlinear function of the enclosed volume, a function which is simply determined by the hypsometry (basin area as a function of height) of a particular basin. This nonlinear term presents the restoring force of a nonlinear oscillator in a second-order ordinary differential equation, which is driven by the external tide and damped by seaward radiation of waves and frictional and form drag in the connecting strait. As the relationship between volume and sea level is in general monotonic, the nonlinear restoring term can be replaced by any other relationship, which is more in accordance with reality, but the linear relationship between surface area and height employed in this study might probably serve as its archetype.

Analysis of this oscillator with linear area–height relationship, has been performed in several limits. In the free case, its solutions can be obtained exactly. Surprisingly, the period of the free mode is restricted to a tiny interval and, moreover, decreases as the nonlinearity increases, in contrast to the increase of period found for classical nonlinear oscillators. Also, the accessible region of phase space, over which stable solutions exist, is limited. Again unlike nonlinear oscillators usually studied in literature, this oscillator has no saddle point. Consequently, when forcing is added, chaos cannot occur in the traditional manner, that is, due to a break-up of the separatrix through a saddle point. Numerical analysis suggests, however, that the Poincaré map does have a saddle point whose separatrices might break-up, resulting in chaos. So far, this seems to be a rare event though, which does not withstand the inclusion of damping.

Indeed, when damping is added, in general only one steady state (limit cycle) is obtained which is phase-locked to the forcing. For some parameter values, however,

multiple steady states exist. Near the primary resonance (forcing frequency close to the Helmholtz frequency) both an amplified and a choked tidal regime may therefore coexist. For forcing periods which are multiples or fractions of the Helmholtz frequency there is one state having the forcing period, as well as a state with a period close to the free period. In this study only a single-frequency forcing has been used. In view of the fact that the tide usually consists of (at least) two frequency components (the semi-diurnal lunar M_2 and solar S_2 tide, related to the spring-to-neap tidal oscillation) it would also be interesting to consider in the future the response to multiple-frequency forcing.

That sloping sides of a 'container' can give rise to a nonlinear response was observed earlier in a study on solitary waves in a channel of arbitrary cross-section (Peregrine 1968). Because of the slope, the cross-sectional area below surface level in this case becomes quadratically related to the height of the free surface. This leads to a reduction of the advective nonlinearity and to an increase in soliton width. Indeed, for strongly varying topography it can turn a soliton into a wave of depression, rather than its usual appearance as a wave of elevation.

In the derivation of the oscillator equation (8) several assumptions have been made that strictly allow the analysis to be applicable only to almost-enclosed basins in which the tidal range is small compared to the mean depth (such as the assumption of a linear sea level slope within the strait). A number of these can be relaxed relatively easily and lead to a more accurate, but slightly more complex, ordinary differential equation for the excess volume. It would be useful to derive and analyse that equation rigorously and see whether that gives a more robust occurrence of chaos that can more easily withstand the inclusion of damping terms.

Finally, the theory derived here is for the Helmholtz-mode only, which imposes some requirements on the configuration of the basin. It leaves one wondering whether incorporation of non-uniform depth (tidal flats) would be relevant to quarter-wavelength resonances in half-open basins, like those in the Bay of Fundy, too.

The author would like to thank Jef Zimmerman for sharing his inspiring thoughts on tidal dynamics in shallow basins, Arjen Doelman for his suggestions concerning the occurrence of chaos in the nonlinear Helmholtz resonator, Huib de Swart for penetrating comments on an earlier draft, and Herman Ridderinkhof, Peter Beerens, Gerard van der Schrier and George Schramkowski for discussions. Rijkswaterstaat (RIKZ) kindly provided tidal elevation and hypsometric data of the Dutch part of the Wadden Sea. Frans Eijgenraam helped in preparing hypsometric curves of this region. This is NIOZ contribution number 3105.

REFERENCES

Abramowitz, M. & Stegun, I. 1964 *Handbook of Mathematical Functions*. Dover.

Boon, J. D. & Byrne, R. J. 1981 On basin hypsometry and the morphodynamic response of coastal inlet systems. *Mar. Geol.* **40**, 27–48.

Carrier, G. F., Shaw, R. P. & Miyata, M. 1971 The response of narrow mouthed harbors in a straight coastline to periodic incident waves. *Trans. ASME* E: *J. Appl. Mech.* **38**, 335–344.

Defant, A. 1961 *Physical Oceanography*, Vol II. Pergamon.

DiLorenzo, J. L. 1988 The overtide and filtering response of small inlet/bay systems. In *Hydrodynamics and Sediment Dynamics of Tidal Inlets* (ed. D. G. Aubrey & L. Weishar), pp. 24–53. Springer.

Elmore, W. C. & Heald, M. A. 1969 *Physics of Waves*. McGraw-Hill.

Fabrikant, A. L. 1995 Harbour oscillations generated by shear flow. *J. Fluid Mech.* **282**, 203–217.

Flather, R. A. & Heaps, N. S. 1975 Tidal computations for Morecombe Bay. *Geophys. J. R. Astron. Soc.* **42**, 489–517.

Friedrichs, C. T. & Madsen, O. S. 1992 Nonlinear diffusion of the tidal signal in frictionally dominated embayments. *J. Geophys. Res.* **97**, 5637–5650.

Garrett, C. 1972 Tidal resonance in the Bay of Fundy and Gulf of Maine. *Nature* **238**, 441–443.

Garrett, C. 1975 Tides in gulfs. *Deep-Sea Res.* **22**, 23–35.

Golmen, L. G., Molvaer, J. & Magnusson, J. 1994 Sea level oscillations with super-tidal frequencies in a coastal embayment of western Norway. *Cont. Shelf Res.* **14**, 1439–1454.

Grebogi, C., Ott, E., Varosi, F. & Yorke, J. A. 1990 Analyzing chaos: a visual essay in nonlinear dynamics. *Energy Sciences Supercomputing*, pp. 30–33.

Green, Th. 1992 Liquid oscillations in a basin with varying surface area. *Phys. Fluids* A **4**, 630–632.

Guckenheimer, J., Myers, M. R., Wicklin, F. J. & Worfolk, P. A. 1992 DSTOOL: a dynamical system toolkit with an interactive graphical interface. *Center for Appl. Math., Cornell Univ.*, pp. 1–64.

Kreeke, J. van de 1988, Hydrodynamics of tidal inlets. In *Hydrodynamics and Sediment Dynamics of Tidal Inlets* (ed. D. G. Aubrey & L. Weishar), pp. 1–23. Springer.

LeBlond, P. H. 1978 On tidal propagation in shallow rivers. *J. Geophys. Res.* **83**, 4717–4721.

Mehta, A. J. & Özsoy, E. 1978 Flow dynamics and nearshore transport. In *Stability of Tidal Inlets* (ed. P. Bruun), pp. 83–161. Elsevier.

Mei, C. C. 1989 *The Applied Dynamics of Ocean Surface Waves.* World Scientific.

Miles, J. W. 1948 Coupling of a cylindrical tube to a half space. *J. Acoust. Soc. Am.* **20**, 652–644.

Miles, J. W. 1974 Harbor seiching. *Ann. Rev. Fluid Mech.* **6**, 17–35.

Miles, J. W. & Lee, Y. K. 1975 Helmholtz resonance of harbours. *J. Fluid Mech.* **67**, 445–464.

Molines, J. M., Fornerino, M. & LeProvost, C. 1989 Tidal spectroscopy of a coastal area: observed and simulated tides of the Lake Maracaibo system. *Cont. Shelf Res.* **9**, 301–323.

Nayfeh, A. H. 1973 *Perturbation Methods.* Wiley-Interscience.

Nayfeh, A. H. & Mook, D. T. 1979 *Nonlinear Oscillations.* Wiley-Interscience.

Okihiro, M., Guza, R. T. & Seymour, R. J. 1993 Excitation of seiche observed in a small harbor. *J. Geophys. Res.* **98**, 18201–18211.

Ostrovskiy, L. A. 1978 Nonlinear internal waves in a rotating ocean. *Oceanology* **18**, 119–125.

Parker, T. S. & Chua, L. O. 1989 *Practical Numerical Algorithms for Chaotic Systems.* Springer.

Peregrine, D. H. 1968 Long waves in a uniform channel of arbitrary cross-section. *J. Fluid Mech.* **32**, 353–365.

Platzman, G. 1972 Two-dimensional free oscillations in natural basins. *J. Phys. Oceanogr.* **2**, 117–138.

Prandle, D. 1991 Tides in estuaries and embayments. In *Tidal Hydrodynamics* (ed. B. B. Parker), pp. 125–152. Wiley and Sons.

Rasband, S. N. 1989 *Chaotic Dynamics of Nonlinear Systems.* Wiley Interscience.

Redfield, A. C. 1961 The tidal system of Lake Maracaibo, Venezuela. *Limnol. and Ocean.* **1**, 1–12.

Ridderinkhof, H. 1988 Tidal and residual flows in the Western Dutch Wadden Sea, I: Numerical model results. *Neth. J. Sea Res.* **22**, 1–22.

Shih, H. H. & Baer, L. 1991 Some errors in tide measurement caused by dynamic environment. In *Tidal Hydrodynamics* (ed. B. B. Parker), pp. 641–671. Wiley and Sons.

Sorensen, R. M. & Seelig, W. N. 1976 Hydraulics of Great Lakes inlet – harbour systems. *Proc. Fifteenth Coastal Engineering Conf., Honolulu, Hawaii*, Vol. 2, pp. 1646–1665. ASCE.

Speer, P. E. & Aubrey, D. G. 1985 A study of non-linear tidal propagation in shallow inlet/estuarine systems. Part II: Theory. *Est. Coast Shelf Sci.* **21**, 207–224.

Stigebrandt, A. 1980 Some aspects of tidal interactions with fjord constrictions. *Est. Coast. Shelf Sci.* **11**, 151–166.

Stommel, H. & Farmer, H. G. 1953 Control of salinity in an estuary by a transition. *J. Mar. Res.* **12**, 13–20.

Zaslavsky, G. M., Sagdeev, R. Z., Usikov, D. A. & Chernikov, A. A. 1991 *Weak Chaos and Quasi-Regular Patterns.* Cambridge University Press.

Zimmerman, J. T. F. 1992 On the Lorentz linearization of a nonlinearly damped tidal Helmholtz oscillator. *Proc. Kon. Ned. Akad. v. Wetensch.* **95**, 127–145.